Brillouin neutron scattering in heavy water: Evidence for two-mode collective dynamics

F. Sacchetti,[1] J.-B. Suck,[2] C. Petrillo,[3] and B. Dorner[4]
[1]*INFM and Dipartimento di Fisica, Universitá di Perugia, I-06123 Perugia, Italy*
[2]*Institute of Physics, Material Research and Liquids, TU Chemnitz, D-09107, Chemnitz, Germany*
[3]*INFM and Dipartimento di Fisica, Politecnico di Milano, I-20133 Milano, Italy*
[4]*Institut Laue Langevin, B.P. 156, F-38042 Grenoble Cedex 09, France*
(Received 21 January 2004; published 4 June 2004)

A high resolution (1.5 meV) inelastic neutron scattering experiment was carried out, aiming at an accurate investigation of the high frequency and low momentum dynamic response in heavy water. The experimental data confirm the existence of a dispersionless mode, besides the ordinary longitudinal collective dynamics. A simplified model, based on the interaction of two vibrational branches, is proposed to interpret the observed features of the dynamic spectra. The validity extent of this scheme is proved by applying it to room temperature neutron and x-ray data, to temperature and pressure dependent x-ray data, and to room temperature neutron data of vibrational density of states. The overall successfull results provided by this model, in conjunction with the combined analysis of the x-ray and neutron data on collective dynamics, enable a deeper insight into the complex mechanisms of the water dynamics and provide a simple phenomenological explanation for the transition from ordinary to fast sound.

DOI: 10.1103/PhysRevE.69.061203 PACS number(s): 47.10.+g, 61.12.Ex, 78.70.Nx, 63.50.+x

I. INTRODUCTION

In a recent paper [1] we reported an accurate inelastic neutron scattering investigation of the collective dynamics of heavy water over an extended dynamic range, which was optimized to study the so-called *fast* sound [2–5]. The experiment in Ref. [1] was carried out on a top performance three-axis spectrometer installed at the High Flux Reactor of the Institut Laue-Langevin (ILL, Grenoble). The results of that investigation revealed that the fast sound could be unambiguously observed by inelastic neutron scattering, and, more interestingly, that a second mode, which is almost dispersionless and behaves like an optic mode, was present. Originally, the dispersionless mode had been observed by inelastic x-ray scattering in the experiment described in Ref. [5]. However, later x-ray scattering measurements [6,7] were interpreted in terms of a single mode with a simple linear dispersion. That seeming contradiction is probably related to the experimental difficulties in observing the dispersionless mode by means of an x-ray probe. Indeed, the intensity associated to this mode is smaller than in the neutron case [1], and its contribution to the x-ray dynamic structure factor can be neglected when analyzing the fast sound. The neutron and x-ray findings were first interpreted by us [1] as an indication for the dispersionless mode being mainly located on the hydrogen (deuterium) atoms, which are much less visible in photon scattering. The conclusion about the presence of an additional mode was also strongly supported by the results of the incoherent neutron scattering experiment in light water reported in Ref. [8], where a well defined peak at the same energy as the dispersionless collective mode was observed in the measured density of states. We emphasize that the experiment of Ref. [8] provides the measurement of the spectrum projected onto the hydrogen nuclei, that is it is a very sensitive probe of the dispersionless mode. The experimental situation is summarized in Fig. 1, where the excitation energies $\hbar\omega(Q)$ associated to the fast sound and to the hydrodynamic isothermal sound are shown versus the wave vector Q and in comparison with the density of states measured over the same energy region. There is a clear correspondence between the peak at $\sim$6 meV in the density of states and the average energy values associated to the dispersionless mode measured in Refs. [1,5].

In the x-ray investigations of Refs. [6,7], the transition from the hydrodynamic *ordinary* sound at low wave-vector transfer to the *fast* sound at large wave-vector transfers was described as due to a structural relaxation process. The occurrence of different dynamic regimes, characterized by fast and ordinary sound velocities, was explained in terms of the relaxation time being larger or shorter than the time scale

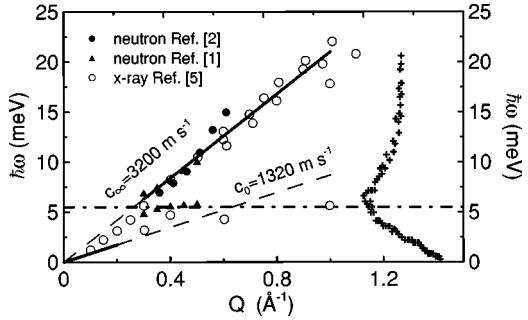

FIG. 1. Summary of the excitation energies observed in water by inelastic neutron scattering experiments (triangles from Ref. [1], dots from Ref. [2]), and by inelastic x-ray scattering experiments (circles from Ref. [5]). The solid lines are the dispersion relations associated to the fast sound (c_∞=3200 ms^{-1}) and to the hydrodynamic sound (c_0=1320 ms^{-1}), with the dashed lines representing the continuations. The dot-dashed line is the dispersionless mode discussed in Ref. [1]. The curve with crosses on the right is the experimental density of states of light water measured in Ref. [8], and shown over the same energy scale. We note the correspondence between the peak in the density of states and the energy associated to the dispersionless mode.

associated to the density fluctuations [9]. The proposed Q-dependent relaxation model was also successfully applied to the interpretation of the pressure- and temperature-dependent x-ray data [6,7]. However, we observe that, despite the satisfactory overall description of the water collective dynamics under different thermodynamic conditions, this model does not take into account the additional intensity at $\sim$6 meV observed in the neutron scattering experiments [1,8].

An alternative description of the complex features of the water dynamics is that provided by the phenomenological interaction model proposed in Ref. [1]. The model is based on the idea that leaving an elementary excitation, with an associated linear dispersion, to interact with a dispersionless mode brings about a splitting of the low-frequency from the high-frequency branches. In Ref. [1] it was shown that the interaction model, although in a rather crude and extremely simplified manner with respect to the richness and complexity of the water dynamics, is able to account for the observed excitations and their dispersion, namely the dispersionless mode and the linearly dispersing acousticlike mode which is associated to a low propagation velocity at low wave-vector transfer and to a high velocity at large wave-vector transfer.

The relaxation and the two-mode interaction schemes are both phenomenological, although a larger degree of complexity remains associated to the relaxation model, and both suggest possible interaction mechanisms of the density fluctuation mode with the system as a whole, as a key to explain the sound propagation in water. In the structural relaxation model, the relaxation time is related to formation and breaking of hydrogen bonds, and the collective mode propagates in a medium which may appear as a solidlike network of molecules or as the ordinary liquid structure, depending on the mode frequency [9]. In the interaction model, the interaction between the collective mode and the system dynamics is essentially confined to the 6-meV band. Under both the interpretation schemes, the interactions of the collective excitation are treated on an empirical basis, although the different microscopic mechanisms lead to a different interpretation of the ordinary to fast sound transition in water. The main difference between the two models remains, in our opinion, the relaxation model not accounting for the dispersionless excitation at $\sim$6 meV, whose existence is proved by the incoherent neutron scattering experiment [8] and by the Brillouin neutron scattering experiment of Ref. [1]. The experimental information available at present is not enough to assess the validity of one model against the other and both could be used as a starting point for interpreting the complex features of the water dynamics.

Additional data come from molecular dynamics simulations that, recently, provided convincing evidence for the presence of two vibrational modes [10], which were related to longitudinal and transverse dynamics in water. Although the simulation result applies to the motion of the center of mass only, it gives further ground to the picture of a two mode dynamics possibly existing in water. Of course, the analysis of the center of mass motion cannot be directly applied to interpret the neutron scattering data. The neutron data are remarkably affected by the deuterium motion, which is likely going to be different from the oxygen motion. In the end, we mention an even more recent molecular dynamics simulation study [11] on the hydration water of a protein crystal, where it was reported that the dynamics of hydration water share many of the spectral features of bulk water. This investigation, demonstrating the central role of the dynamics of hydration water, proved, once again, the importance of accessing to a deeper understanding of the water dynamics, either in itself or for the impact it has in fields like life science [11].

Here, we present the results of a different inelastic scattering experiment on heavy water, again using neutrons which are more sensitive to the presence of the additional dynamics at 6 meV. The experiment was designed to confirm and more deeply investigate the presence of the dispersionless mode and its interaction with the acousticlike mode. Therefore it was carried out at higher energy resolution and with better statistics. Referring to the data collected previously [1], we judged that 1.5-meV energy resolution was adequate to determine the dynamic structure factor with sufficiently high accuracy. Indeed, such a resolution is quite adequate to deal with the rather broad features of the water spectra and it has the advantage of being comparable with-that employed in the high resolution x-ray experiments. This would enable a meaningful comparison of neutron and x-ray data, despite the different analytic functions describing the instrument resolution.

II. EXPERIMENT

The preferred choice for carrying out the present experiment was the three-axis neutron spectrometer IN1 on the hot source at the ILL, where inelastic scans were collected in the fixed final wave-vector configuration, namely $k_F=6.2$ Å^{-1} as selected by a vertically focusing (400) Cu crystal analyzer. The low d-spacing (331) vertically focusing Cu monochromator was mounted. Very tight collimations of 25′, 20′, 20′, and 30′ were employed from the reactor to the detector. This spectrometer configuration, in combination with the low background from an evacuated flight path around the sample, 1 m in diameter, enabled the collection of high quality data down to 1° scattering angle, and, despite the tight collimations, a sufficiently high intensity was available at the sample. The elastic energy resolution, corresponding to such a configuration, was determined by inelastic scans on a vanadium standard at the exchanged wave vectors $Q=0.2$ Å^{-1} and $Q=0.4$ Å^{-1}, and it turned out to be 1.5 meV. Considering the rather high value of final energy, i.e., 80 meV, a relative energy resolution better than 2% was quite a good achievement. The kinematic region $(Q,\hbar\omega)$ spanned in the present experiment is sketched in Fig. 2 in comparison with that accessible to the previous neutron experiment [1], and together with the dispersion relations associated to the collective modes, as measured in Ref. [1]. This figure shows that the $(Q,\hbar\omega)$ region covered by the two experiments was appropriate to investigate the propagation of collective excitations in water.

The sample was D_2O, 99.99% deuterium rich, with a large size matching the full cross section of the incoming beam and an optimal thickness appropriate to reduce the

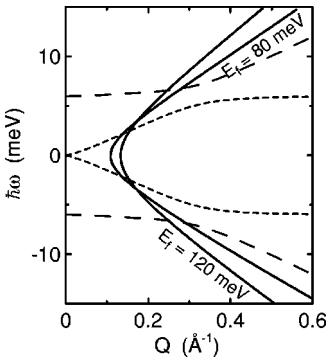

FIG. 2. Kinematic region $(Q,\hbar\omega)$ accessible to the present investigation (80-meV final neutron energy and 1° scattering angle) and to the neutron experiment of Ref. [1] (120-meV final neutron energy and 1° scattering angle). The dashed lines are the dispersion relations associated to the collective excitations in water, as described in Ref. [1].

multiple scattering (MS) contribution in the scattered intensity. The geometric characteristics of the sample container had been optimized in the experiment of Ref. [1], and hence the same sample cell was used for the present measurements. It was a slab shaped (8 cm $\times$ 4 cm $\times$ 0.8 cm) pure aluminium cell with a window thickness of 0.5 mm. To reduce MS, the same honeycomb shaped cadmium grid, successfully used in Ref. [1], was mounted inside the cell. Each hexagonal hollow of the grid had an edge length of 0.6 cm and the same depth as the cell thickness, i.e., 0.8 cm.

The intensity scattered from the heavy water sample was measured at 293 K at seven wave-vector transfer values, namely $Q=0.2$, 0.25, 0.3, 0.35, 0.4, 0.45, and 0.5 Å^{-1}. Careful measurements of all possible background contributions were carried out. This was necessary to accomplish good quality data after the background subtraction, especially on the tails of the scattering function. Indeed, at a given Q, the highest energy transfers, which correspond to the tails, are attained at the smallest scattering angles, that is in configurations of the analyzer-detector next to the incident beam and resulting in a higher background. The scattering from the empty cell was measured at the same Q values as the sample, while the background produced outside the sample region was measured at $Q=0.25$ and 0.3 Å^{-1} with the sample substituted by a highly absorbing 2-mm-thick Cd plate. Additional measurements at $Q=0.3$ Å^{-1} were collected on both the sample and the empty cell after removing the cadmium honeycomb grid. The purpose of these measurements was that of having an experimental check for the subtraction of the MS contribution.

As anticipated, the elastic resolution of the instrument was measured by inelastic scans at $Q=0.2$ and 0.4 Å^{-1} on a 2-mm-thick vanadium plate inserted into the sample cell. The vanadium spectra, which are shown in Fig. 3, were very well reproduced by the theoretical resolution function calculated according to the standard Cooper and Nathans procedure [12] for the specific three-axis configuration. The present experimental resolution was very well described by a Gaussian function with 1.5 meV full width at half maximum (FWHM).

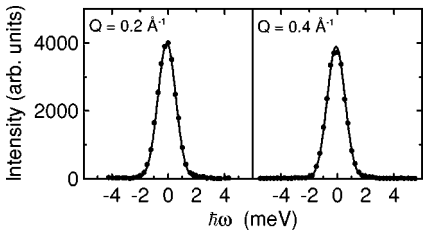

FIG. 3. Intensity of the vanadium standard versus energy transfer, measured at $Q=0.2$ and 0.4 Å^{-1} (dots). The solid lines are Gaussian curves with 1.5 meV FWHM describing the instrument resolution function [12].

The procedure applied to correct the experimental data, which schematically consists of monitor normalization, background subtraction, MS and attenuation corrections, and absolute normalization was described in detail in Ref. [1]. Here, we briefly comment only on the measurements designed to test the accuracy of the MS subtraction. The MS contribution was obtained by a simulation procedure and the quality and reliability of the calculation were checked against the experimental data of the sample measured with and without the honeycomb grid. Indeed, the effect of the Cd grid is that of decomposing the whole available volume into many almost cylindrical little volumes and its insertion inside the cell amounts to an MS reduction that the simulation must account for properly. The intensity scattered from the water sample in the two configurations, with and without the grid, was simulated at the wave-vector transfer $Q=0.3$ Å^{-1}. The difference between the two calculated intensities was convoluted with the four-dimensional $(\mathbf{Q},\omega)$-dependent resolution function of the spectrometer and normalized to the energy-integrated intensity scattered without the Cd grid. The resulting curve is compared with the corresponding experimental difference in Fig. 4, where it is apparent that the MS simulation accounts for the measured data very well. This result is even more notable considering that no free adjustable parameters are introduced to work out the comparison.

Having assessed the reliability of the MS simulation, extended calculations were carried out to correct the data at

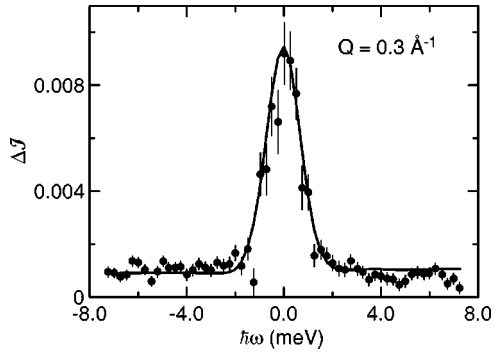

FIG. 4. Intensity from the water sample collected with $(\mathcal{I}^g)$ and without $(\mathcal{I})$ the honeycomb Cd grid (see text). The relative intensity difference at the kth energy point, $\Delta\mathcal{I}=(\mathcal{I}_k-\mathcal{I}_k^g)/\Sigma_k\,\mathcal{I}_k$, is shown versus the energy transfer at $Q=0.3$ Å^{-1}. Dots: experimental data. Full line: curve calculated with the present MS simulation.

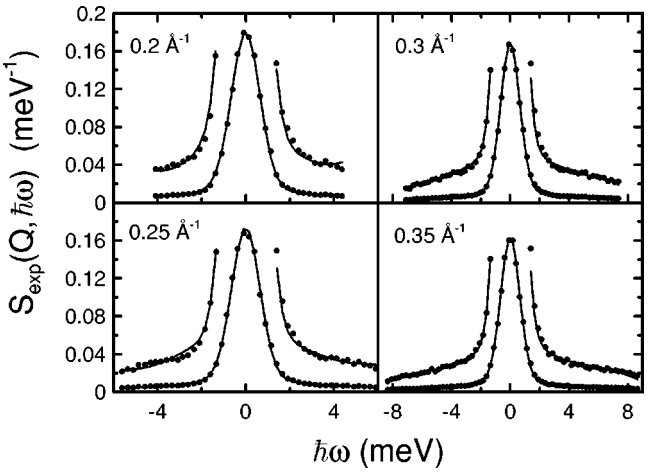

FIG. 5. Dynamic structure factor $S_{exp}(Q\hbar\omega)$ of heavy water versus energy transfer and at the lowest wave vectors measured in the present neutron experiment. The experimental data (dots) and the best-fitting curves (lines), calculated according to the two-mode interaction model described in the text, are shown also on an expanded scale.

every wave-vector transfer Q. The MS intensity was convoluted with the spectrometer resolution function and it was subtracted from the measured data. The resulting intensity was normalized imposing the condition that the integral of the experimental dynamic structure factor $S_{exp}(Q,\hbar\omega)$ be equal to $[4\pi b^2 S(Q)+\sigma_{inc}]/[4\pi b^2+\sigma_{inc}]$, $S(Q)$ being the static structure factor [13], b and σ_{inc} the coherent scattering length and the incoherent cross section of the bound molecule. This normalization procedure produced the same results, within the experimental errors, as the standard normalization to vanadium.

An overall view of the experimental dynamic structure factor is presented in Figs. 5 and 6 versus energy and at the wave-vector transfers of the measurements. A close inspection of the figures reveals that, apart from a resolution limited quasielastic peak, purely inelastic features are present. The energy resolution of this experiment, which is sharper than that of Ref. [1], enables us to better define the dispersion of the collective mode and to investigate the contribution below the extended wings of the quasielastic peak, as discussed in the next section.

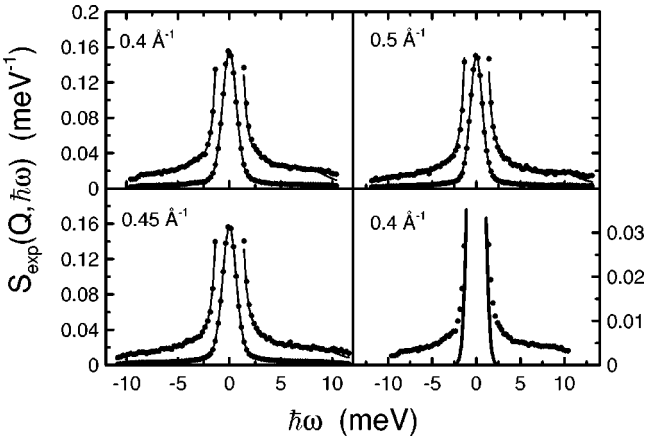

FIG. 6. Same as Fig. 5, but at the largest wave vectors measured in the present neutron experiment. The bottom right panel shows, on an expanded scale, the experimental data (dots) in comparison with the resolution function (solid line) at $Q=0.4$ Å^{-1}, to emphasize the effect of the instrument resolution on the side structures of the inelastic peak.

III. DATA ANALYSIS

The quantitative analysis of the present data proceeded from the two-mode model introduced in Ref. [1] to describe the data there collected. Due to the complexity of the water spectrum, which resembles that of hexagonal ice (Ih) [14], the two-mode model has an overall validity which is confined to the energy band below 15–20 meV. Over the window 0–15 meV, the main feature of the energy spectrum is the ~6-meV peak for liquid water and an optic phonon at about the same energy for ice Ih. Higher frequency modes are present, however, their contributions to the propagating longitudinal density fluctuations in liquid water are not in the energy window here investigated. By the present model, we are not suggesting that all the optic modes in ice Ih collapse into just one opticlike mode in the liquid, but we are exploiting at most the experimental evidence of a density of states peaked at ~6 meV. Therefore the assumption of a single dispersionless mode should be regarded as representative of a set of closely spaced modes falling within the same energy band, the width of which is brought about by the envelope of the modes or by some intrinsic damping mechanism. Over the investigated frequency region, the dispersionless mode can be expected to interact with acoustic modes.

Quite schematically, the model amounts to the simplifying assumption that the inelastic dynamics of water at high frequency and low momentum can be described by two mutually interacting modes: an almost dispersionless mode and an acousticlike mode. As a result of the interaction, the linear dispersion remains associated with a low velocity c_0 at low wave vectors and a high velocity c_∞ at large wave vectors. We observe that similar predictions about the velocity come out from the study of Ref. [15] on the fast sound in a crystalline system made by disparate-mass components, which has the theoretical support of the linearized hydrodynamics.

According to the model, the calculated dispersion relations $\omega_\pm(Q)$ associated to the two interacting modes turn out to be [1]

$$\omega_\pm^2(Q) = \frac{\omega_a^2 + \omega_0^2 \pm \sqrt{(\omega_a^2 - \omega_0^2)^2 + 4\beta^2}}{2},$$

where ω_0 is the frequency of the dispersionless mode, $\omega_a = c_\infty Q$ is the dispersion of the unperturbed acousticlike mode and $\beta(Q)$ describes the coupling between the modes. As described in Ref. [1], a sensitive choice for $\beta(Q)$ is $\beta(Q) = Q\,\beta_0 \exp(-\lambda Q)$, that is, the interaction is assumed to increase linearly at low Q and to decay exponentially at large Q values. An appealing characteristic of this model is the simple and straightforward interpretation of the transition from the ordinary sound, associated to the low-

Q velocity c_0, to the *fast sound*, associated to the high-Q velocity c_∞. Indeed, in the low-Q limit one has

$$\omega_+(Q) = \omega_0$$

and

$$\omega_-(Q) = Qc_0 = Q\sqrt{c_\infty^2 - \frac{\beta_0^2}{\omega_0^2}}. \quad (1)$$

It is interesting to observe that, within this model, the unperturbed sound velocity is c_∞, that is the velocity associated to the fast sound. On the other hand, the alternative interpretation of the transition from ordinary to fast sound in terms of viscous relaxation [6,9] refers to c_0 as the unperturbed mode velocity with the fast sound resulting from the relaxation of the sound mode through its interaction with a random field inside the system.

The experimental dynamic structure factor $S_{exp}(Q,\hbar\omega)$, as obtained from the data reduction procedure described in Sec. II, consists of the cross-section-weighted sum of the dynamic structure factor and its self-term. The empirical two-mode model was exploited to describe the purely inelastic coherent component of the response related to the collective mode, while the quasielastic scattering due to both coherent and incoherent cross sections was modeled by Lorentzian functions. The optimal choice for the model function $S_{mod}(Q,\omega)$ to be fitted to the experimental data, after convolution with the resolution function of the spectrometer, was then

$$S_{mod}(Q,\omega) = S_0^L(Q,\omega) + S_1^L(Q,\omega) + S_-(Q,\omega) + S_+(Q,\omega) \quad (2)$$

with

$$S_0^L(Q,\omega) = \frac{\hbar\omega/k_BT}{1-\exp(-\hbar\omega/k_BT)}\frac{a_0(Q)}{\pi}\frac{\Gamma_0(Q)}{\omega^2+\Gamma_0^2(Q)},$$

$$S_1^L(Q,\omega) = \frac{\hbar\omega/k_BT}{1-\exp(-\hbar\omega/k_BT)}\frac{a_1(Q)}{\pi}\frac{\Gamma_1(Q)}{\omega^2+\Gamma_1^2(Q)},$$

$$S_-(Q,\omega) = \frac{1}{1-\exp(-\hbar\omega/k_BT)}\frac{a_+(Q)\Gamma_+(Q,\omega)}{[\omega^2-\omega_+^2(Q)]^2+\Gamma_+^2(Q,\omega)},$$

$$S_+(Q,\omega) = \frac{1}{1-\exp(-\hbar\omega/k_BT)}\frac{a_-(Q)\Gamma_-(Q,\omega)}{[\omega^2-\omega_-^2(Q)]^2+\Gamma_-^2(Q,\omega)},$$

$\Gamma_0(Q)=DQ^2/(1+\tau DQ^2)$, D being the measured self-diffusion coefficient of water [16] ($D=2.2\times10^{-5}$ cm^2 s^{-1}) and τ the residence time with the value given in Ref. [17]. $\Gamma_1(Q)$, $\Gamma_\pm(Q,\omega)$, $a_0(Q)$, $a_1(Q)$, and $a_\pm(Q)$ were left as free parameters. With this choice, the number of free parameters of the fit was rather large and to reduce it we used the same assumption as in Ref. [1], namely the damping function $\Gamma_\pm(Q,\omega)$ given by $\hbar\Gamma_\pm(Q,\omega)=\alpha_\pm Q\omega$.

We comment that, as in Ref. [1], the purely inelastic contributions are fitted by two damped harmonic oscillators (DHOs). Although the use of two DHO could appear rather restrictive, it is just an easy to handle tool which provides good quality empirical fits to the experimental data. Moreover, in the two-mode model, the meaningful quantities are the frequencies $\omega_\pm(Q)$, which represent the effective dispersion relations. They are obtained from the set of the best fit parameters accordingly to the model and to the numerical procedure described in the following.

To prove the capabilities of this fitting model, the data measured in the present experiment were fitted simultaneously with those collected in the previous neutron experiment [1] using the same set of parameters. The only exception was allowing the amplitude parameters $a_0(Q)$ and $a_\pm(Q)$ to be different for the two sets of data, which reflects the different experimental conditions of the two measurements. The overall fit of the $S_{exp}(Q,\hbar\omega)$ data by means of Eq. (2) was found to be of satisfactory quality for all the measured wave-vector transfers and for both sets of data. Indeed, the reduced χ^2 values were about the same, namely 1.6 for the present set of data and 1.8 for the data of Ref. [1]. The number of free parameters of the fit can be further reduced by observing that $\Gamma_1(Q)$ shows a negligibly small, if any, Q dependence. Then, a meaningful assumption was consistent with keeping $\Gamma_1(Q)=\Gamma_1$, that is constant. With this position, the fit of all the measured neutron spectra was carried out using seven nonlinear Q-independent parameters, namely Γ_1, c_∞, ω_0, β_0, λ and $\alpha_\pm$, and the four amplitudes $a_0(Q)$, $a_1(Q)$, and $a_\pm(Q)$, which are linear fitting parameters. The number of nonlinear parameters could be further reduced to five by using the condition of Eq. (1) with c_0 bound to be equal to the value measured at ultrasound frequency, i.e., 1320 ms^{-1}, and by assuming $\alpha_-(Q)=\alpha_+(Q)$. In the end, since the data of Ref. [1] were not sensible to the presence of the broader Lorentzian $S_1^L(Q,\omega)$ in the fit, because of the rather coarse resolution of that experiment (2.6 meV), the same values for $a_1(Q)$ were assumed for the two sets of data. The following best fit values were obtained for the Q-independent parameters: $\hbar\Gamma_1=1.5\pm0.1$ meV, $\hbar c_\infty=20.0\pm0.5$ meV/Å^{-1}, i.e., $c_\infty=3040\pm80$ m/s, $\hbar\omega_0=6.0\pm0.5$ meV, i.e., $\omega_0/2\pi=1.45\pm0.15$ THz, $\lambda=3.3\pm0.5$ Å, and $\alpha_\pm=120\pm1.0$ meV Å. We observe that the combined fit of the present and the Ref. [1] data provided parameters with values identical, within the quoted errors, to those found in Ref. [1]. This result gives

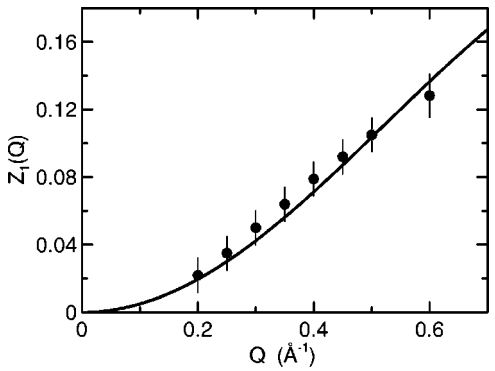

FIG. 7. Wave-vector dependence of the strength integral $Z_1(Q)$ of the broad Lorentzian component $S_1^L(Q,\omega)$ of the neutron fit. The continuous line is the model function $f=f_0[1-\sin(Qd)/(Qd)]$ fitting the $Z_1(Q)$ data (see text).

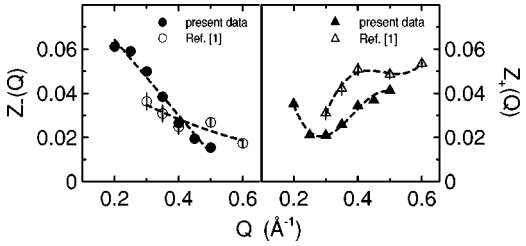

FIG. 8. Wave-vector dependence of the strength integrals $Z_-(Q)$ and $Z_+(Q)$ associated to the (−) and the (+) vibrational modes, and described by $S_-(Q,\omega)$ and $S_+(Q,\omega)$ in the fit to the present neutron data (filled symbols). The results obtained in the neutron experiment of Ref. [1] are also shown by open symbols, for comparison purposes. The dashed lines are a guide to the eye.

support to the reliability of the whole procedure. The only difference between the present fitting model and that of Ref. [1] was the addition of the second broader Lorentzian to model the quasielastic peak. Such a Lorentzian was necessary to obtain a good quality fit of the present data, which are at higher resolution although spanning a slightly smaller dynamic range. It was not required to fit the previous data, because of their lower resolution, although it was compatible with them.

The weigths of the four components which comprise the dynamic structure factor, and the analysis of the mode strengths can be obtained by calculating the following integrated intensities:

$$Z_{0/1}(Q) = \int_{-\infty}^{+\infty} d\omega\, S^L_{0/1}(Q,\omega),$$

$$Z_{\pm}(Q) = \int_{-\infty}^{+\infty} d\omega\, S_{\pm}(Q,\omega).$$

The values here obtained for the Z integrals agree, within normalization errors, with those calculated in Ref. [1]. As to their Q dependence, $Z_1(Q)$ is an increasing function of the wave vector Q, as apparent from Fig. 7. This behavior, coupled to the Q independence of Γ_1 over the present Q range, suggests that the quasielastic scattering in water at low Q is mostly accounted for by the two contributions modeled by the Lorentzian functions of the fit. The first contribution, described by the narrow Lorentzian function $S^L_0(Q,\omega)$ with associated width $\Gamma_0(Q)$, can reasonably represent the self-diffusion of water molecules, whereas the second much broader Lorentzian $S^L_1(Q,\omega)$ embodies the dynamics of fast processes, possibly related to confined motions, as it is suggested by the value of the Q-independent width $\Gamma_1 = 2.28 \times 10^{12}$ s^{-1}. The range of the conjectured confined motion can be deduced by fitting the experimental $Z_1(Q)$ data with the low-Q limit of the simple model function $f(Q) = f_0[1 - \sin(Qd)/(Qd)]$, f_0 and d free parameters. We found a distance $d \sim 4$ Å, that is, a size of the confinement region comparable with the size of the tetrahedral network of the water molecules.

The integrals $Z_{\pm}(Q)$ are shown in Fig. 8 as a function of Q

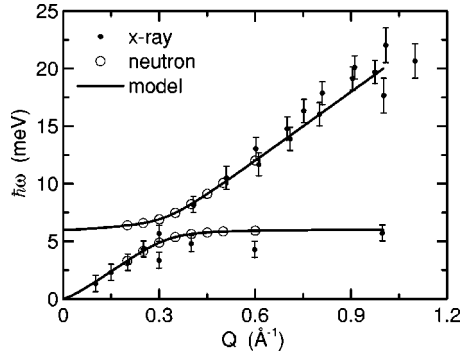

FIG. 9. Dispersion relations of the collective excitation in water. The continuous lines are the dispersion curves associated to $\hbar\omega_-(Q)$ and $\hbar\omega_+(Q)$ obtained by a global fit of the two-mode interaction model to the neutron data of the present and Ref. [1] experiments. The neutron data, that necessarily lie on the calculated curves, are identified by open circles. The x-ray data resulting from the experiment and the analysis described in Ref. [5] are also shown for comparison purposes (dots).

for the present and the old set of neutron data, and, notwithstanding the quite different experimental conditions, a substantial overall agreement between the two sets of corresponding data is apparent. As to the Q dependence of $Z_{\pm}(Q)$, it is roughly found that $Z_-(Q)$ is a decreasing function of Q, while $Z_+(Q)$ is an increasing one. It is interesting to note that the sum of $Z_-(Q)$ and $Z_+(Q)$ is smaller than the overall contribution expected for coherent scattering from the static structure factor estimate. This proves that coherent scattering also is contributing to the quasielastic peak, as expected over the present wave-vector region, and in agreement with the observation of a remarkable quasi elastic peak in the always fully coherent x-ray measurements.

Finally, the dispersion curves associated to the fitting parameters $\hbar\omega_-(Q)$ and $\hbar\omega_+(Q)$, which again compare quite well with the results quoted in Ref. [1], are shown in Fig. 9 for sake of completeness. In this figure, the results of the x-ray experiment of Ref. [5], obtained by the fit there described, are also shown. Although the fitting procedures applied to the analysis of the x-ray and the neutron data are different, Fig. 9 emphasizes the excellent agreement between the results of the two experiments.

IV. VALIDATION OF THE INTERACTION MODEL AGAINST THE LITERATURE DATA

The analysis performed so far has been applied to treat the data of two coherent neutron scattering experiments, both carried out at room temperature. The simple model of two coupled modes accounts simultaneously for all the features observed in the spectra. Nonetheless, the validity of such a model should be scrutinized against a wider set of experimental data on the atomic dynamics in water. In the following, we apply the present model to the analysis of the extended set of x-ray inelastic scattering data reported in Ref. [6] and of the density of states data measured by incoherent inelastic neutron scattering in liquid light water and reported in Ref. [6].

A. Analysis of the x-ray data at 277 K

The large body of inelastic x-ray scattering data reported in Ref. [6] represents an ideal ground to test the capability of the present model to interpret the features of the water dynamics. A first set of x-ray data are those measured at 277 K and normal pressure, that is in thermodynamic conditions quite similar to those of the neutron scattering experiments. The same dynamic behavior, apart from a probably small isotopic effect, is expected to be observed in the two experiments, once the different probe-to-sample coupling is taken into account. The direct coupling of neutrons to the atomic nuclei, via a short range potential, makes them a perfectly suited probe of the dynamics of nuclei, whilst this is observed via the electron-nucleus coupling when probing the system with photons. In water, the electron cloud is mostly centered on the oxygen atom and the dynamics probed by x-ray scattering is largely dominated by the oxygen motion, that is it is closely related to the motion of the center of mass of the water molecule. The large coherent cross section of deuterium makes, on the other hand, the neutron scattering experiment in heavy water especially sensitive to the deuterium dynamics.

We carried out a new fit to the x-ray data at 277 K and normal pressure, reported in Ref. [6], by using the model function given in Eq. (2). To make the x-ray versus neutron comparison independent of data-reduction related effects, the x-ray dynamic structure factor was normalized as in the neutron case, that is imposing the integral of $S_{\mathrm{exp}}(Q,\hbar\omega)$ be equal to the static structure factor $S(Q)$. The accurate x-ray static structure factor measured in Ref. [18] was used. The so normalized $S_{\mathrm{exp}}(Q,\hbar\omega)$, after convolution with the experimental resolution function of the x-ray instrument [6], were fitted to the x-ray data.

On the assumption that the same dynamics is probed by the two experiments, the fit was performed by keeping the parameters Γ_1, ω_0, c_∞, $\alpha_\pm$, and λ fixed and equal to the values provided by the neutron fit. These constraints amount to leaving the amplitudes $a_0(Q)$, $a_1(Q)$, and $a_\pm(Q)$, which are linear parameters, as the only free parameters of the x-ray fit. This ultimately reflects the different coupling of the two probes to the system. The results are shown in Fig. 10 where the high quality of the fit is apparent. We observe that the broad Lorentzian function $S_1^L(Q,\omega)$ of the model function [Eq. (2)], which was necessary to accurately fit the neutron data, had a negligible effect on the fit of the x-ray data. Indeed, a fit of the same quality as that shown in Fig. 10 was obtained neglecting this contribution. This result is brought about by the extended wings of the x-ray almost-Lorentzian resolution function which mask possible contributions from the broad Lorentzian $S_1^L(Q,\omega)$ of the model.

The relative weight of the various contributions to the x-ray dynamic structure factor was given by the Z integrals calculated with the parameters resulting from the fit to the x-ray data. Smooth dependences were obtained for $Z_0(Q)$ and $Z_1(Q)$. In Fig. 11, $Z_-(Q)$ and $Z_+(Q)$, resulting from the integration of the x-ray data, are shown as a function of Q. The observed decreasing trend of $Z_-(Q)$ vs Q is consistent with the behavior expected from a continuous transition of the corresponding $(-)$ mode from acousticlike to opticlike, while the opposite increasing trend of $Z_+(Q)$ reflects the transition of the $(+)$ mode from an opticlike to an acousticlike character.

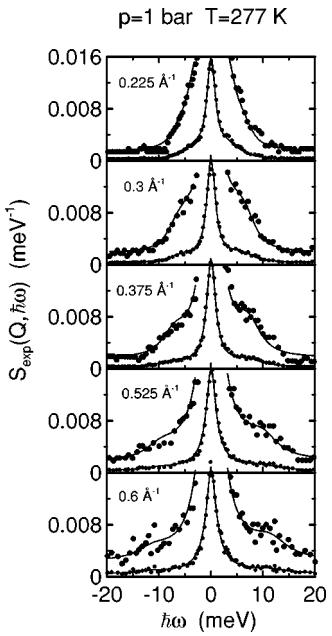

FIG. 10. Dynamic structure factor $S_{exp}(Q,\hbar\omega)$ of light water at $T=277$ K and normal pressure, versus energy transfer and at the wave vectors measured in the x-ray experiment reported in Ref. [6]. The solid lines are the best-fitting curves resulting from the fitting of the x-ray data by means of the present interaction model, with all the nonlinear parameters already fixed by the companion fit to the neutron data (see text). The data and the calculated curves are shown also on an expanded scale.

The overall results obtained by applying the present interaction model to the analysis of the x-ray data, which are mostly sensitive to the dynamics of the water molecule center of mass, are not in contradiction with the simple picture of two interacting modes, one with a well-defined acousticlike character and the other with opticlike characteristics.

To discuss photon and neutron data on a quantitative base, we exploited the representation of the dynamic structure factor by means of the three partial atom-atom correlation functions which can be defined in water, namely $S_{OO}(Q,\omega)$, $S_{OH}(Q,\omega)$, and $S_{HH}(Q,\omega)$. The coherent contribution to the

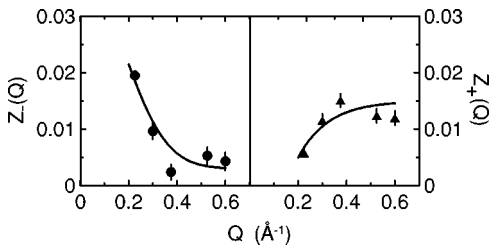

FIG. 11. Wave-vector dependence of the strength integrals $Z_-(Q)$ and $Z_+(Q)$ associated to the $(-)$ and $(+)$ vibrational modes, described by $S_-(Q,\omega)$ and $S_+(Q,\omega)$ in the fit to the x-ray data [6]. The solid lines are a guide to the eye.

dynamic structure factor probed in neutron scattering experiments, i.e., $S^{(n)}(Q,\omega)$, can be written as

$$S^{(n)}(Q,\omega) = \frac{\sum_{\alpha\beta} b_\alpha b_\beta S_{\alpha\beta}(Q,\omega)}{2b_D^2 + b_O^2}, \tag{3}$$

where the sums run over the atoms of the water molecule and b_D=6.67 fm and b_O=5.45 fm are the scattering lengths of deuterium and oxygen, respectively. The three partial correlation functions have similar weights and the corresponding dynamic correlations are expected to equally contribute to the neutron cross section. In the case of x-ray scattering, since the motion of each nucleus has a complex and distributed effect on the electron cloud, only an approximate version of Eq. (3), with validity confined to low wave vectors, can be written. The dynamic structure factor $S^{(x)}(Q,\omega)$, which is always coherent at low wave-vector transfers, is then written as

$$S^{(x)}(Q,\omega) = \frac{\sum_{\alpha\beta} Z_\alpha Z_\beta S_{\alpha\beta}(Q,\omega)}{2Z_H^2 + Z_O^2}, \tag{4}$$

where Z_H and Z_O are the atomic numbers of hydrogen and oxygen, respectively. $S^{(x)}(Q,\omega)$ is dominated almost completely from the oxygen-oxygen term, while the oxygen-hydrogen term contributes by about 25% and the hydrogen-hydrogen term by less than 2%. Although Eq. (4) has a limited validity, it suggests that x-ray scattering experiments probe mainly the oxygen contribution, with the other two correlation functions hardly detectable. These characteristics make the comparison of neutron and x-ray scattering experiments extremely appealing, since a wealth of information about the water dynamics can be obtained from the simultaneous and common analysis of the data.

The independent knowledge of the Z integrals for both neutron and x-ray data can be exploited to distinguish the dynamic features related to oxygen and hydrogen atoms. Indeed, under the assumption of a solidlike behavior of the system, the integrals can be written as

$$Z_\pm(Q) = \{2n[\omega_\pm(Q)] + 1\}\frac{\hbar Q^2}{\omega_\pm(Q)}\sum_{\alpha\beta} w_\alpha w_\beta F_\alpha^\pm(Q) F_\beta^\pm(Q), \tag{5}$$

where $n(\omega)$ is the Bose factor, the sums run over the hydrogen and the oxygen atoms, the weights w_α are related to neutron and photon scattering amplitudes through

$$w_\alpha = \frac{f_\alpha}{\sqrt{\sum_\alpha f_\alpha^2}}$$

with f_α equal to b_α for neutrons and to Z_α for photons. The partial structure factors $F_H^\pm(Q)$ and $F_O^\pm(Q)$, associated to the two modes and distinct for the two atoms, can be obtained from the combined analysis of neutron and x-ray data through Eq. (5). The structure factors so deduced are shown in Fig. 12. The hydrogen structure factor was found to be larger than that of oxygen, as expected. In particular, $F_H^\pm(Q)$ exceeds $F_O^\pm(Q)$ by about a factor 3 on average, that is by a value which is close to the square root of the oxygen to hydrogen (deuterium) mass ratio. Although the structure factors were obtained under several approximations, including the use of data measured on light and heavy water, the overall trend here found is perfectly meaningful. The observed wave-vector transfer dependence of the structure factors is generally simple, and, together with the prevailing hydrogen contribution at large wave vectors, gives further account for the scarce visibility of the dispersionless opticlike mode by x-ray scattering.

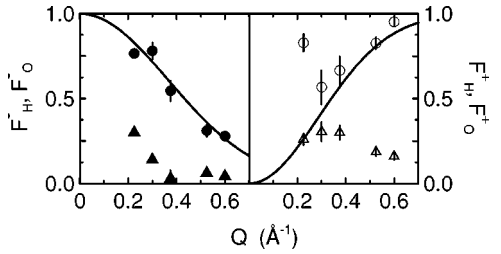

FIG. 12. Wave-vector dependence of the structure factors of hydrogen (filled and open circles) and oxygen (filled and open triangles), separately associated to the low-lying (−) and the upper (+) vibrational modes. The solid lines are analytic expressions for the hydrogen structure factors associated to the two modes.

B. Analysis of temperature- and pressure-dependent x-ray data

The analysis applied so far to the x-ray data at 277 K and normal pressure can be equally applied to the temperature- and pressure-dependent x-ray data, also reported in Ref. [6]. In particular, the data at the thermodynamic conditions summarized in Table I were selected for the analysis. Since the set of parameters deduced from the fit to the room temperature data cannot be used here, the fit of the complete set of x-ray data was carried out by letting all the parameters freely change. The same normalization as for the normal condition experiment was applied. The quality of all the fits was found to be comparable with that at 277 K and normal pressure. The most relevant parameters of the fit, namely c_∞ and ω_0, and the corresponding χ^2 values, are also listed in Table I.

The results show that at 3000 bars and 277 K there is a small effect on c_∞, although the ratio c_∞/c_0 is equal to 1.58 ± 0.04, whereas it is equal to 2.13 ± 0.05 at 277 K and normal pressure. This finding is consistent with the increase of the interaction parameter β_0 from 98 ± 3 to 106 ± 3 meV^2 Å when the pressure is increased from 1 to 3000 bars. The resulting picture is that an increase of pressure at fixed temperature, which in turn produces an increase of density, gives rise to an increase of the interaction between the two modes, while the energy of the mode is only marginally affected. This behavior can be explained by observing that the water dynamics at short wavelength is dominated by the local atomic arrangement, which does not appreciably change on changing the density over the present limited range (less than 10%). On the other hand, the increase of density produces a corresponding increase of c_0.

TABLE I. Thermodynamic temperature (T) and pressure (p) conditions associated to the inelastic x-ray scattering measurements of Ref. [6], here reanalyzed by applying the two-mode interaction model (see text). The mass density ρ and the hydrodynamic sound velocity c_0, corresponding to the (T,p) points, after Ref. [6], are also listed. The parameters c_∞, associated to the fast sound velocity, and $\hbar\omega_0$, that is the energy of the dispersionless mode, obtained by the present fit to the x-ray data are reported together with the corresponding χ^2 values.

T (K)	p (bars)	ρ (g cm^{-3})	c_0 (m s^{-1})	c_∞ (m s^{-1})	$\hbar\omega_0$ (meV)	χ^2
277	1.00	1.000	1430±20	3040±80	6.0±0.5	1.68
277	3010	1.109	2020±40	3200±80	6.0±0.5	1.17
273	900	1.042	1567±6	3040±80	6.0±1.0	0.90
300	1.00	0.977	1510±20	2740±80	5.0±1.0	0.88
333	400	1.000	1627±8	2580±80	3.2±1.0	0.90
373	1020	1.001	1742±7	2430±80	3.2±1.0	0.76
413	1530	0.993	1801±2	2280±80	4.0±1.0	1.17
453	1550	0.965	1760±10	2050±80	4.0±1.0	0.80

The dependence of c_0 on the compressibility, which is an extended property of the system, reduces the effects of the local atomic arrangement. The interaction between the two modes, which accounts for the transition from c_0 to c_∞, also can be considered an extended property of the system and hence it is expected to depend on the density. A similar trend for c_∞ was observed in Ref. [7], where the data were analyzed using a single DHO. This is an indication that the behavior of c_∞ is, as expected, only marginally model dependent and seems to be an intrinsic feature of the water dynamics.

Further information can be gained from the temperature-dependent data. As an example, the results of the present fit to the x-ray data are compared with the experiment in Fig. 13. The excellent quality of all these fits suggests that the interaction model can be successfully applied over the whole thermodynamic range which was investigated by x-ray scattering, and not only to treat the neutron data at normal conditions. An effect worth to note is the appreciable decrease,

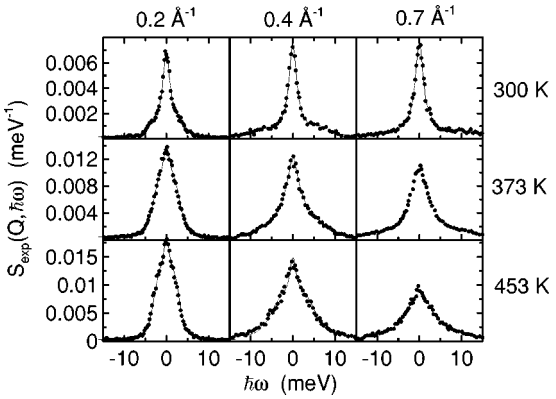

FIG. 13. Dynamic structure factor $S_{exp}(Q,\hbar\omega)$ of light water versus energy transfer, at constant density and at three temperature values. The x-ray experimental data (dots) are from Ref. [6]. The solid lines are the best-fitting curves to the x-ray data obtained by applying the present interaction model.

from 6 to 3.5 meV, of ω_0 when increasing the temperature at almost constant density. A neutron scattering experiment devoted to the study of the hydrogen spectrum over the same thermodynamic conditions would be extremely desirable to verify the shift of the peak towards lower energy.

C. Hydrogen density of states

The inelastic incoherent neutron scattering experiment on light water, presented in Ref. [8], can be interpreted by means of the two-mode model with parameters determined by the fits discussed so far. Indeed, the density of states, which is measured by the experiment of Ref. [8], can be calculated by using the $\omega_\pm(Q)$ dispersion relations and the experimental atomic structure factors associated to the two modes, as obtained from the Z integrals through Eq. (5). This procedure is appropriate to treat a quasiharmonic solid in the incoherent approximation. Actually, the incoherent approximation is also a suitable scheme to describe the dynamics of the light water sample because of the large incoherent cross section of the proton, which dominates the response. In the harmonic solid, the H-weighted density of states of an sth eigenmode is given by

$$g_s(\omega) = \sum_{BZ} \delta(\omega - \omega_s(\mathbf{q}))[F_H^s(\mathbf{q})]^2, \tag{6}$$

where the sum runs over the $\mathbf{q}$ values within the first Brillouin zone and $\omega_s(\mathbf{q})$ is the eigenfrequency of the $(s,\mathbf{q})$ mode. Equation (6) can be applied to a liquid system by making, however, some assumptions. First of all, a damping mechanism of the crystal modes has to be brought in, which for the present interaction model is contained into the $S_\pm(Q,\omega)$ functions and results into

$$g_\pm(\omega) = \sum_{\mathbf{q}} \frac{S_\pm(\mathbf{q},\omega)}{Z_\pm(\mathbf{q})}[F_H^s(\mathbf{q})]^2 \tag{7}$$

with $g_\pm(\omega)$ the densities of states associated with the $\hbar\omega_\pm(Q)$ modes. To carry out the sum over the Brillouin zone in the

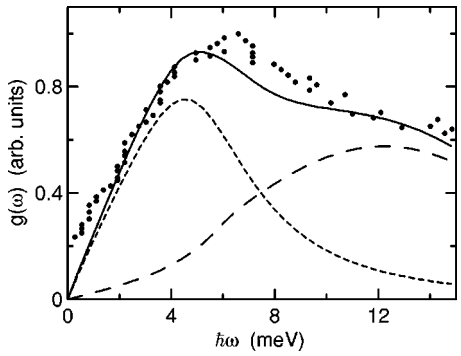

FIG. 14. Density of vibrational states in light water versus energy. The experimental neutron data (dots) from Ref. [8] are shown in comparison with the curve (solid line) calculated in the framework of the interaction model (see text). The two contributions to the calculated density of states, originating from the $\hbar\omega_-(Q)$ mode (short-dashed line) and the $\hbar\omega_+(Q)$ mode (long-dashed line) are also plotted to emphasize the different wave-vector dependence of the two contributions.

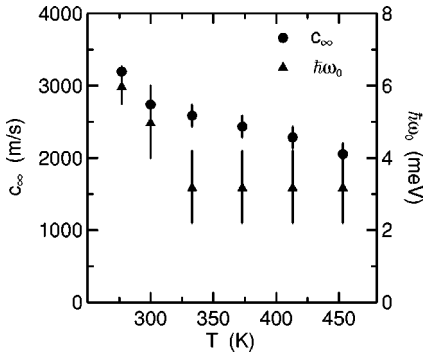

FIG. 15. Temperature dependence of the fitting parameters c_∞ (dots) and $\hbar\omega_0$ (triangles) obtained by fitting the present interaction model to the temperature-dependent x-ray data of Ref. [6].

liquid system, we made the ansatz that the Brillouin zone is approximated by a spherical region with a radius equal to $Q_0/2$, Q_0 being the wave vector corresponding to the first maximum of the static structure factor, which is ~1.97 Å in heavy water [13]. The sum in Eq. (7) was then converted into the spherical integral from 0 to $Q_0/2$, and the hydrogen structure factor F_H^S was approximated by means of the simple interpolation function shown in Fig. 12. The so calculated density of states is shown in Fig. 14 against the experimental data of Ref. [8], which were normalized by a scale factor to make the comparison clear.

Considering the approximations contained in this procedure, which heavily relies on the solid state approach outlined in Eqs. (6) and (7), the resulting agreement between the curve calculated with the present model and the experimental data is excellent. We believe that the observed agreement is a further, and rather convincing, argument in support of the interaction model as an interpretation scheme of the water dynamics, which favors a solidlike picture of the collective modes in liquid water, over the high frequency range explored by neutron and x-ray techniques. In Fig. 14 the specific contributions arising from the two modes used in the present model of water dynamics are also plotted. The decomposition of the density of states shows that the peak observed in the experimental data should be linked to $\hbar\omega_-(Q)$. The $\hbar\omega_-(Q)$ branch contributes mainly over the Q region close to $Q_0/2$, where it approaches $\hbar\omega_0$. As a consequence, the dispersionless mode appears to play an important role for interpreting the peak observed in the energy spectrum. The good agreement observed in Fig. 14 indicates also that there is only a very small effect due to the mass difference (hydrogen vs deuterium) on the position of the peak located at ~6 meV. Therefore the dispersionless mode should be attributed to the water molecule complex and hence to the local tetrahedral arrangement present in liquid water at room temperature. Finally, we remark that these conclusions have been achieved by making use of both neutron and x-ray data which were both necessary for refining the parameters of the present model.

V. CONCLUSION

The primary conclusion we can draw from the present analysis is that the interaction model provides an adequate description of the whole set of spectra available from neutron and x-ray inelastic scattering experiments in the energy region below 20 meV. The most appealing result is the determination of the hydrogen and oxygen structure factors, a result made possible by the combined use of x-ray and neutron data within the same model, and which enables a deeper insight into the water dynamics at an atomic level. Within a solidlike model, the atomic structure factors provide an estimate of the water density of states in good agreement with that measured by incoherent neutron scattering. Unfortunately, there are no molecular dynamics simulations providing the independent dynamics of both hydrogen and oxygen in water, and therefore suitable for a comparison with the results of the present work. Carrying out such a comparison would represent a stringent test for the details of the intermolecular potentials employed in the simulations.

The validity of the interaction model to describe the water dynamics in thermodynamic conditions different from the standard ones has been proved by the successful fit of the temperature and pressure dependent x-ray data. A systematic trend of the fitting parameters as a function of temperature at *almost* constant density was found. In particular, a systematic decrease of both c_∞ and ω_0 when increasing the temperature was observed. This trend is visible in Fig. 15 where the two parameters are shown as a function of the temperature. It is interesting to note that the ratio between the two parameters is almost constant. These characteristics suggest that the frequencies of the two modes are related to the same intermolecular force field, which softens on increasing the temperature, i.e., a behavior consistent with a solidlike interpretation of the high frequency dynamics is suggested. We note also that the interaction parameter β_0, as determined from the x-ray data, rapidly decreases from 106 ± 3 meV^2 Å at 277 K to 42 ± 3 meV^{2}Å at 333 K and then more slowly down to 28 ± 3 meV^2 Å at 453 K. This trend is probably related to a more localized nature of the opticlike mode, brought about by the progressive disentanglement of the long range hydrogen bond network, occurring at higher temperatures. A further effect is related to the growth of defects and interstitial

water molecules in the hydrogen bond network with increasing pressure, which disrupts the tetrahedral local structure and weakens the hydrogen bonds. Indeed, the decrease of both c_∞ and ω_0 was observed with increasing the temperature at constant density, that is with increasing also the pressure. This behavior is in agreement with the picture sketched above, which was established by the recent accurate molecular dynamic simulation of Ref. [19].

In summary, we want to remark once more the empirical nature of the interaction model used to rationalize the entire large set of experimental observations coming from neutron and x-ray measurements. The model has the merit of pointing out the fundamental features of the water dynamics out of the extremely complex spectra in a rather intuitive fashion. Notwithstanding the appealing simplicity of this solid-like model, we remind that its validity should not be extended beyond the limits of an empirical realm. Indeed, the complexity of the water dynamics cannot be fully accounted for by a limited set of phenomenological parameters. We also believe that the investigation of other prototypical hydrogen-bonded liquids would help to assess the ability of the interaction model in describing a class of systems and not simply water.

[1] C. Petrillo, F. Sacchetti, B. Dorner, and J.-B. Suck, Phys. Rev. E **62**, 3611 (1999).
[2] J. Teixeira, M. C. Bellissent-Funel, S. H. Chen, and B. Dorner, Phys. Rev. Lett. **54**, 2681 (1985).
[3] F. J. Bermejo, M. Alvarez, S. M. Bennington, and R. Vallauri, Phys. Rev. E **51**, 2250 (1995).
[4] G. Ruocco, F. Sette, U. Bergmann, M. Krisch, C. Masciovecchio, V. Mazzacurati, G. Signorelli, and R. Verbeni, Nature (London) **379**, 521 (1996).
[5] F. Sette, G. Ruocco, M. Krisch, C. Masciovecchio, R. Verbeni, and U. Bergmann, Phys. Rev. Lett. **77**, 83 (1996).
[6] G. Monaco, A. Cunsolo, G. Ruocco, and F. Sette, Phys. Rev. E **60**, 5505 (1999).
[7] M. Krisch, P. Loubeyre, G. Ruocco, F. Sette, A. Cunsolo, M. DAstuto, R. LeToullec, M. Lorenzen, A. Mermet, G. Monaco, and R. Verbeni, Phys. Rev. Lett. **89**, 125502 (2002).
[8] M.-C. Bellissent-Funel, S. H. Chen, and J.-M. Zanotti, Phys. Rev. E **51**, 4558 (1995).
[9] G. Ruocco and F. Sette, J. Phys.: Condens. Matter **11**, R259 (1999).
[10] M. Sampoli, G. Ruocco, and F. Sette, Phys. Rev. Lett. **79**, 1678 (1997).
[11] M. Tarek and D. J. Tobias, Phys. Rev. Lett. **89**, 275501 (2002).
[12] M. J. Cooper and R. Nathans, Acta Crystallogr. **23**, 357 (1967).
[13] M. -C. Bellissent-Funel, *Hydrogen Bonded Liquid, Vol. 329 of NATO Advanced Study Institute Series C: Mathematical and Physical Sciences*, edited by J. C. Dore and J. Teixeira (Kluwer, London, 1991), pp. 117–128.
[14] B. Renker, in *Physics and Chemistry of Ice*, paper presented at the Symposium on the Physics and Chemistry of Ice, held in Ottawa, Canada, 14-18 August 1972, edited by E. Whalley, S. J. Jones, and L. W. Gold (Royal Society of Canada, Ottawa, 1973), pp. 82–86; Phys. Lett. **30A**, 493 (1969).
[15] E. Enciso, N. G. Almarza, M. A. Gonzalez, F. J. Bermejo, R. Fernandez-Perea, and F. Bresme, Phys. Rev. Lett. **81**, 4432 (1998).
[16] K. T. Gillen, D. C. Douglass, and M. J. R. Hock, J. Chem. Phys. **57**, 5117 (1972).
[17] J. Teixeira, M.-C. Bellissent-Funel, S. H. Chen, and A. J. Dianoux, Phys. Rev. A **31**, 1913 (1985).
[18] A. H. Narten, M. D. Danford, and H. A. Levy, Discuss. Faraday Soc. **43**, 97 (1967).
[19] F. Sciortino, A. Geiger, and H. E. Stanley, Nature (London) **354**, 218 (1991).